Testing a Coupled Ice–Mixed-Layer Model Under Subarctic Conditions

MARIE-NOËLLE HOUSSAIS

Laboratoire d'Océanographie Dynamique et de Climatologie, Université Paris 6, Paris, France

(Manuscript received 15 July 1986, in final form 21 July 1987)

ABSTRACT

A one-dimensional oceanic mixed-layer model has been coupled with a thermodynamic sea ice model in order to study the seasonal cycle of ice–ocean interaction in the subarctic ocean. The ice thickness is assumed constant and only variations of ice compactness under the effect of the atmospheric and oceanic heat fluxes are considered. The mixed-layer model allows prediction of the rate of entrainment, mainly as the result of the penetrative buoyancy-driven convection. Both heat and salt conservation equations are included so that the respective efficiency, with regard to vertical mixing, of brine rejection below the ice and intense surface cooling in open water can be compared.

The model has been run for ten years on a zonal vertical section across the Greenland Sea. The annual entrainment–retreat cycle of the mixed layer is well reproduced with maximum depths occurring in late winter, even down to the bottom at some locations near the ice edge. Surface cooling is found to be a more efficient mechanism, compared with brine rejection, in driving winter convection: as a result, mixed-layer deepening slows down as soon as surface freezing occurs and the mixed-layer depth tends to decrease as the ice concentration increases westward. The zonal profiles of the mixed-layer temperature are in good agreement with the seasonal climatological distributions. Finally, the model produces realistic ice concentration distributions in winter. The underestimated summer ice concentrations probably result from the oversimplified ice thermodynamics, since the ice distribution appears to be sensitive to the value prescribed as the ice thickness. A more detailed ice thickness distribution is expected to improve the estimation of the ice melting rate.

1. Introduction

The mechanisms involved in atmosphere–ice–ocean interaction in polar regions remain, at the present time, one of the major problems to be elucidated in order to improve our understanding of the polar, and hence global, climate. Of particular interest is the investigation of the seasonal signal which turns out to be the perequisite to a reliable prediction of the longer time scales (multiyear) of the climate variability. In the Arctic, major field experiments (AIDJEX 75–76, MIZEX 83–84) have concentrated on this seasonal aspect, but at the same time, a special effort is required in the parameterization of the energy transfers and mixing processes occurring both in the atmosphere and in the ocean boundary layers.

The present paper describes the numerical framework and the preliminary results of an oceanic mixed-layer model which has been tested under subarctic atmospheric conditions characterized by possible drastic cooling or freezing at the ocean surface. As far as the signature of deep convection events is found in mixed-layer deepening, the prediction of a variable depth mixed layer is particularly relevant in the subpolar ocean. Among the mechanisms proposed to explain the advent of oceanic deep convection, neither sinking of surface or intermediate waters by interleaving along isopycnal surfaces (Metcalf, 1955), nor double diffusion (Carmack and Aagaard, 1973) seem to provide a satisfying answer. On the other hand, vertical mixing produced in high latitudes by surface atmospheric cooling or salt rejection from growing ice has been identified as a possible driving mechanism. Studies carried out in the Weddell Sea (Killworth, 1979; Martinson et al., 1981) demonstrated that mixing has to be associated with a preconditioning like a topographic effect or a baroclinic instability of the large-scale field (Gascard and Clarke, 1983) in order for overturning to reach down to the bottom.

According to the preceding remarks, the seasonal deepening-retreat cycle of the mixed layer is viewed here as more like the response to the surface thermodynamic forcing rather than the result of shear instability associated with the wind-driven currents (Pollard et al., 1973). The assumption seems reasonable in view of the considerable depths (several hundred meters) the mixed layer can reach in winter in the subpolar ocean. Robinson et al. (1979) have reported thicknesses of up to 900 meters for the convective layer in the southern Greenland and Labrador Seas. Consequently, even if mechanical production is involved in the first stage of the entrainment process, the rapid dissipation of this energy with depth suggests that its influence

Corresponding author address: Dr. Marie-Noelle Houssais, L.O.D.Y.C., UA 1206 CNRS, Universite Paris 6, 4 Place Jussieu, 75252 Paris Cedex 05 France.

becomes negligible as the mixed layer deepens further down. Accordingly, local turbulence models (see Mellor and Yamada, 1982, for a review), in which the main mechanism generating the turbulence available for entrainment of deeper layers is the mean velocity shear, are of little help. Significant mean current velocities are usually restricted to the Ekman layer, which only covers the very upper part of the mixed layer in winter. In comparison, vertically integrated models of convectively driven mixed layers (Kraus and Turner, 1967) have produced interesting results in climatic simulations. The preceding assumption also provides a justification for considering a seasonally varying thermodynamic forcing (based on monthly mean values) and discarding the effect of shorter time scales mainly involved in mechanical forcing (wind stress or ice-water stress) fluctuations. It should be noted that in doing this, the effects of the submonthly (especially diurnal) variability in buoyancy forcing are neglected altogether.

In the particular case of high-latitude conditions, mixed-layer models have to be coupled with an active or prescribed sea-ice cover (Kim and Gates, 1980; Manabe and Stouffer, 1980). In such coupled ice–ocean models, temperature which is usually selected as the determinative parameter for describing the vertical structure in open water is usually replaced by salinity, which evolves according to the salt flux released from the ice cover. In the model proposed, the alternate occurrence of ice-covered and open water surface conditions is taken into account through the coupling of the ocean surface layer with a fully interactive thermodynamic ice model including variable ice concentrations. It is thus possible to investigate the relative influence of the different driving mechanisms responsible for the mixed-layer deepening or retreat. Buoyancy forcing effects induced by brine rejection or fresh water supply from the ice are to be compared with radiative and heat forcing (especially intense winter cooling) available from the atmosphere in open water areas. This is done by considering both temperature and salinity as prognostic variables of the ocean surface-layer model.

In previous coupled ice–mixed-layer models (Lemke and Manley, 1984; Pollard et al., 1983) the evolution of the ice cover is generally independent from the underlying ocean. Instead, ice melting and freezing rates are calculated from observations or from a thermodynamic budget of the ice including some prescribed oceanic heat flux. When more sophisticated models of sea ice including ice advection, and even ice interaction (Hibler, 1979) are used, the oceanic mixed layer is either nonexistent or parameterized as a fixed slab (Parkinson and Washington, 1979; Hibler, 1980) with no possible entrainment or retreat. Even if inclusion of ice dynamics improves the prediction of the ice distribution by allowing a net imbalance of fluxes to occur locally over a seasonal cycle, the heat transfer from the deeper layers is also a very important process which, in such models, is poorly reproduced. Estimated as a residual in the one-dimensional prognostic mixed-layer model of Pollard et al. (1983), it was found unrealistically large, demonstrating the need for a better parameterization of the exchange with the deeper layers.

Even in a three-dimensional ice–ocean model where a simple parameterization of the vertical diffusion is used instead of an explicit prediction of the mixed-layer depth (Hibler and Bryan, 1987), interaction of the surface layer with the deeper ocean appears important, in addition to the combined effect of ice and ocean advection, to adequately estimate the local ice melting-freezing balance and the subsequent location of the ice edge.

In comparison with these studies, emphasis is given in the present work to local processes by coupling a very simple one-dimensional ice model, where ice dynamics is neglected, with a prognostic mixed-layer model in which both heat and salt entrainment fluxes are calculated. The model has been tested along a zonal slab in the Greenland Sea where a wide range of ice concentrations (including open water) together with areas which are well-conditioned with regard to deep convection, are expected to be found.

2. Model description

The numerical framework consists of a sea ice model which predicts the modification of the surface forcing at the top of the mixed layer according to the thermodynamic response of the ice cover to atmospheric and oceanic fluxes, and a bulk mixed-layer model. Simulation results with this one-dimensional coupled model, where no advection or horizontal diffusion are included, are presented in section 3.

a. The mixed-layer model

The mixed-layer model predicts the bulk temperature and salinity, T_m and S_m, of the assumed fully turbulent well-mixed ocean surface layer (e.g., see Niiler and Kraus, 1977). When neglecting the molecular diffusion across the base of the mixed layer, $z = -h_m$, the one-dimensional conservation equations for heat and salt, vertically integrated from $z = -h_m$ to the surface, are written in the form (see Fig. 1)

$$h_m \frac{\partial T_m}{\partial t} + [T_m - T(-h_m)] \frac{\partial h_m}{\partial t} = -(\overline{w'T'})_0 - \int_{-h_m}^{0} \gamma I_s \exp(\gamma z) dz \quad (1)$$

$$h_m \frac{\partial S_m}{\partial t} + [S_m - S(-h_m)] \frac{\partial h_m}{\partial t} = -(\overline{w'S'})_0 \quad (2)$$

where S is the salinity in ‰. The surface turbulent fluxes are expressed as functions of the forcings at the atmosphere- or ice–ocean interfaces (see section 2c for details):

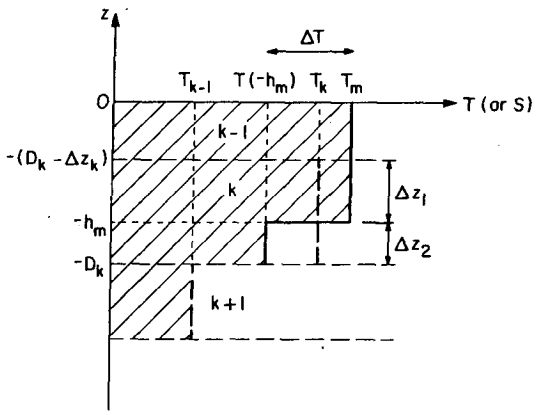

FIG. 1. Schematic diagram of the mixed layer. Its base, $z = -h_m$, is located within the kth of the 13 levels describing the ocean stratification. The vertical salinity distribution is assumed to follow the same step-like profile as the temperature.

$$-(\overline{w'T'})_0 = \begin{cases} -\dfrac{F_{AW}}{\rho_w c}, & \text{if no ice} \\ \dfrac{k_w}{\rho_w c}(T_f - T_m), & \text{if ice} \end{cases} \tag{3}$$

$$-(\overline{w'S'})_0 = \begin{cases} S_m(E-P), & \text{if no ice} \\ H_0\dfrac{\partial A}{\partial t}\dfrac{\rho_I}{\rho_w}(S_m - S_I), & \text{if ice.} \end{cases} \tag{4}$$

In (3) F_{AW} represents the atmosphere radiative and heat fluxes reaching the ice-free ocean surface and T_f is the freezing point. In (4) E and P are respectively the evaporation and precipitation rates, ρ_I and S_I the ice density and salinity; $H_0\partial A/\partial t$ is the rate of change of ice volume (see details of the ice model). The second term on the right-hand side of (1) accounts for the penetrating part of the solar radiation I_s.

There are no velocity equations in the model. Assuming a vertically uniform velocity profile within the mixed layer does not seem reasonable for the special case of subarctic conditions where, as long as no surface freezing occurs, intense surface cooling, combined with very weak ambient stratification, helps in building a deep winter mixed layer. In this case, the vertical scale of the mean velocity variations as predicted by boundary layer theories is expected to be much less than the mixed-layer depth. This indicates that the rate of production of the mean shearing motion by the wind can be higher than the rate of its destruction by turbulent mixing, a fact which is in contradiction with the bulk model assumption of no shear production of turbulence in the interior of the mixed layer. However, as said earlier, due to the forcing time scale considered here, which is much longer than the inertial period, shear production cannot be accounted for.

The system (1)–(2) is not closed because the estimation of the entrainment fluxes between the mixed layer and the underlying ocean:

$$-(\overline{w'T'})_{-h_m} = \frac{\partial h_m}{\partial t}[T_m - T(-h_m)] \tag{5}$$

$$-(\overline{w'S'})_{-h_m} = \frac{\partial h_m}{\partial t}[S_m - S(-h_m)] \tag{6}$$

requires the determination of the entrainment velocity $w_e = \partial h_m/\partial t$. Following Niiler and Kraus (1977), the entrainment equation is obtained from a parameterization of the different terms in the vertically integrated turbulent kinetic energy equation:

$$w_e(q^2 + \Delta B h_m) = \underset{A}{2mu_*^3} + \underset{B}{\frac{h_m}{2}((1+n)(\overline{b'w'})_0} \underset{C}{-(1-n)|(\overline{b'w'})_0|)} + \frac{g\alpha}{\rho_0 c} I_S \Big\{ \underset{D}{h_m[1+\exp(-\gamma h_m)]} - \underset{E}{\frac{2}{\gamma}[1-\exp(-\gamma h_m)]} \Big\} \tag{7}$$

where the effect of the velocity shear and of downward momentum radiation by internal waves through the mixed-layer base have been neglected; ΔB is the buoyancy jump at the base of the mixed layer. Term C which parameterizes the mechanical energy input due to wind or ice stress is always a source term for turbulence. It is expressed as a function of the friction velocity $u_* = (|\tau|/\rho)^{1/2}$ where $|\tau|$ is the wind stress magnitude.

The other possible source term in (7) is D, which can be alternatively positive or negative depending on the sign of the surface buoyancy flux

$$(\overline{b'w'})_0 = g[\alpha(\overline{w'T'})_0 - \beta(\overline{w'S'})_0] \tag{8}$$

where $\alpha = -\rho^{-1}(\partial\rho/\partial T)$ and $\beta = \rho^{-1}(\partial\rho/\partial S)$ are the expansion coefficients of the density with respect to temperature and salinity.

Although the significance of each of the terms in (7) can be found in Niiler and Kraus (1977), some remarks concerning its application to the present particular case have to be made. As buoyancy is assumed here to play the prominent role in the entrainment phase, a detailed estimation of the time–space distribution of C was not felt necessary during such periods. Accordingly, a constant and uniform value was selected for u_* regardless of the presence of ice. Taking a uniform u_* is equivalent to assuming, as usually recognized, that the ice surface compared to the ocean surface is characterized by a larger drag coefficient and that, in addition, the amount of mechanical energy absorbed by the ice exactly compensates for the excess of energy given by the wind at its surface (e.g., see Roed and O'Brien, 1983). Since C is therefore essentially involved in the maintenance of the turbulence levels during periods of mixed-layer retreat, the simplification to a uniform u_* only affects the prediction of the summer mixed-layer thickness.

In fact, (7), in case of negative w_e, turns out to be only a diagnostic equation for h_m, setting $w_e = 0$, instead of providing a real prediction of h_m.

Both production terms, C and D when positive, are subject to dissipation rates which, following Lemke and Manley (1984) and Kim and Gates (1980), insure an exponential decay of the kinetic energy production as h_m increases:

$$n = \exp(-h_m/h_c)$$

$$m = p\exp(-h_m/h_w)$$

where p is equal to 3 and typical values for h_c and h_w have been respectively set to 100 and 20 m. Therefore, for large values of h_m, dissipation can make C and D very small. At the same time, term E keeps a decreasing negative value as it is proportional to h_m, the e-folding scale γ^{-1} for I_s being in this case smaller than h_m. The situation then occurs where there is no more entrainment but no retreat either, as the penetrating solar radiation is felt down to the mixed-layer base. The term I_s is therefore responsible for a reduction of the turbulent potential energy by a larger amount than the amount created by convection. This situation is quite unusual at midlatitudes where E is generally a source term dominated by the penetration depth γ^{-1} and characterized by smaller magnitudes than the two other source terms.

The efficiency of the entrainment process is also controlled by the buoyancy jump ΔB (term B), which determines the amount of work against stratification to lift denser water upward. Again, in case of a convective layer penetrating deep into the underlying weakly stratified ocean, this jump is often so small that the flux of turbulent energy across the mixed-layer base (term A), usually assumed negligible, is no more to be neglected compared to (B). In such a case, A keeps the term in brackets on the left-hand side of (7) close to a lower limit value which has been scaled according to Kim (1976), by

$$q^2 = 9\ \max(10^{-4}\,\mathrm{m^2\,s^{-2}}, u_*^2)$$

b. Treatment of the pycnocline

The buoyancy jump ΔB appearing in (7) is an approximation by a step-like profile of the vertical density structure within the pycnocline. This is an alternative to a continuously stratified pycnocline which would remain undisturbed in case of a nonpenetrative convection model (see, e.g., Killworth, 1979) or would be modified under penetrative convection (Lemke and Manley, 1984). However in both cases, an analytical shape usually taken as exponential has to be assumed and the associated parameters calibrated according to appropriate datasets. To avoid this problem, simple discontinuous profiles for temperature and salinity using a multilevel formulation were chosen to describe the underlying stratification. This solution allows the pycnocline temperature and salinity, $T(-h_m)$ and $S(-h_m)$, and consequently the buoyancy jump ΔB to vary depending on the depth of the penetrative convection. Although the comparative study carried out by Solomon (1973) in the Arctic does not provide a definite conclusion concerning the different types of convection, a fully penetrative convection, as considered for example by Kraus and Turner (1967), was given preference over a nonpenetrative mixing because it conserves potential energy as buoyancy is removed at surface and denser water is entrained at the mixed-layer base.

However, a problem of potential energy conservation arises when the mixed layer retreats to a shallower depth since the model has only two variables, $T(-h_m)$ and $S(-h_m)$, to describe the pycnocline. As soon as a new depth h'_m is diagnostically estimated from (7), it is no longer possible to keep track of the detailed structure of the new pycnocline. Therefore, to insure potential energy conservation in addition to heat and salt conservation, a small change in T_m and S_m is allowed as in Adamec et al. (1981) so that the new mixed layer and pycnocline temperatures (and similarly, salinities) are given by

$$T'_m = T(-h_m) + \frac{[T_m - T(-h_m)]h_m(D_k - h_m + D_m)}{D_k D_m}$$

$$T'(-h_m) = T(-h_m) + \frac{[T_m - T(-h_m)]h_m(h_m - D_m)}{D_k(D_k - D_m)} \quad (9)$$

where

$$D_k = \sum_{l=1}^{k} \Delta Z_l$$

$$D_m = \max(h'_m, D_k - \Delta Z_k).$$

c. The thermodynamic sea ice model

The ice model has many features in common with that of Roed (1984). Essentially, ice thickness time changes are considered negligible when compared with ice compactness changes. As mentioned by Roed, this crude approximation is motivated by observations of typical marginal ice zone conditions (as encountered in the subpolar ocean) where, due to the collision and breakup of individual floes lateral melting or freezing seemed to predominate over vertical melting or freezing.

The vertical thermodynamic budget of an ice floe of unit area and constant thickness H_0 allows the prediction of the ice compactness A (percentage of ice-covered area) by compensating any imbalance in the vertical fluxes by a change in the ice mass. When downward fluxes are considered negative, the budget can be written

$$L_I H_0 \frac{\partial A}{\partial t} = A(F_{AI} - F_{WI}) + (1 - A)[F_{AW}(T_f) - F_{WA}] \times H[\max(T_f, T_c) - T_m] \quad (10)$$

where H is the Heaviside step function and L_I the volumetric latent heat of fusion for sea ice; F_{AI} is the sum of atmospheric radiative and turbulent heat fluxes reaching the ice surface at temperature T_I; F_{WI} and F_{WA} are the oceanic heat fluxes, respectively, at the ice bottom and immediately below the open ocean surface.

On the right-hand side of (10), the first term is the contribution of the ice-covered area to the rate of change of ice mass due to an imbalance between fluxes at the top and bottom of the ice floes. The second term is the contribution due to an imbalance between fluxes at the air–sea interface; T_c is a critical temperature for the underlying mixed layer below which surface freezing can occur. Since F_{AW} is usually positive at high latitudes, this critical temperature is higher or equal to T_f according to

$$T_c = T_f + \frac{F_{AW}(T_f)}{k_w}. \tag{11}$$

Equation (11) follows from a simple parameterization of F_{WA} as

$$F_{WA}(T_s) = k_w(T_m - T_s) \tag{12}$$

and from the statement that just as surface freezing is initiated, the heat fluxes at the ocean surface must balance each other so that $F_{WA}(T_f) = F_{AW}(T_f)$. In (12) T_s is the ocean surface temperature and $k_w = 270$ W K^{-1} m^{-2} is the ocean heat transfer coefficient. The idea here is that ice formation does not necessarily require that the whole mixed layer be at the freezing point, but only that a very thin surface sublayer have its temperature T_s equal to the freezing point. A possibly distinct surface sublayer has also been used by Killworth (1979) in his time-dependent model in which distinction is made between three ice cases B, C, D and two no-ice cases A, E. In fact, unless the whole mixed-layer temperature reaches the freezing point, the present ice model is always supplied by an oceanic heat flux F_{WI} coming from the warmer underlying mixed layer and transferred through the surface sublayer whatever its actual temperature is. Accordingly, the surface temperature T_s is not to be predicted as an explicit variable of the model, and the freezing condition in (10) can be expressed as

$$H(T_f, T_s) = H[\max(T_c, T_f), T_m]$$

The same kind of parameterization as (12) is also used for F_{WI}:

$$F_{WI} = k_w(T_m - T_f) \tag{13}$$

The surface fluxes F_{AW} and F_{AI} are expressed as the sum of the radiative, sensible and latent heat fluxes, using bulk aerodynamical formulas:

$$F_{A\binom{W}{I}} = (1 - \alpha_{\binom{W}{I}})F_S - I_S + \epsilon_{\binom{W}{I}}F_L + \epsilon_{\binom{W}{I}}\sigma T_{\binom{m}{I}}^4 + \rho_a C p_a U_a C_s (T_{\binom{m}{I}} - T_a) + \Lambda_{\binom{W}{I}}E \tag{14}$$

where $\binom{W}{I}$ are subscripts for water or ice and F_S, F_L, U_a and T_a are prescribed climatological values for the flux of shortwave solar radiation, longwave atmospheric radiation, the wind speed and the surface air temperature. The constant Λ is the volumetric latent heat of evaporation or sublimation, α the albedo, ϵ the emissivity, and C_s a surface drag coefficient. The exact calculation of F_{AI} requires knowing the surface ice temperature T_I. Here T_I is diagnostically calculated noting that, as long as it is smaller than T_f, the conductive flux through the ice floe has to balance the atmospheric flux at the top surface of the floe:

$$k_I(T_f - T_I) = F_{AI} \tag{15}$$

where $k_I = 1$ W K^{-1} m^{-2} is the ice heat transfer coefficient.

In all the calculations discussed above, the ice thickness is set equal to a constant value H_0 which has been selected so as to keep A mostly within the range [0,1]. In the rare cases where A would exceed unity, then H_0 is increased and A kept equal to 1. Apart from the two diagnostic variables T_I and T_s, the model has only one prognostic variable, the ice volume.

3. Application of the model to the Greenland Sea

a. Simulation conditions

Equations (1), (2) and (7) with the help of (3), (4) and (9) for the ocean, and Eq. (10) with the help of (11), (13), (14) and (15) for the ice, have been solved in order to perform a simulation of the seasonal cycle of ice–ocean interaction in the Greenland Sea. The domain is a zonal vertical slab at latitude 75°N extending from 20°W to 20°E (Fig. 2). This slab is about 1200 km long and 3.6 km deep at its deepest point. Topography is included on the 80 point × 13 level grid with a 15 km horizontal resolution.

The atmospheric forcing was taken from climatological data (Vowinckel and Orvig, 1970). Monthly mean values of F_S, F_L, E, P and U_a, T_a were interpolated to daily values over an annual cycle that was repeated every year. The values of F_S, F_L, E and P are considered spatially uniform over the domain while T_a, and hence the sensible heat flux, is allowed to vary horizontally according to the monthly maps of air temperature given by Vowinckel and Orvig. Also, the ocean/ice thermal radiation and the sensible heat flux are subject to the time–space changes of the surface temperature $T_{\binom{m}{I}}$ predicted by the model. The zonal winter and summer distributions of the resulting heat gain at the ocean surface for an ice distribution corresponding to the equilibrium state are shown in Fig. 3. As the forcing is strongly dominated by the sensible heat flux in open water, there is a rapid drop in the magnitude of the winter surface cooling at the ice edge location (5°W). According to the zonal variation of the surface air–ocean temperature difference in winter, the surface heat flux keeps a rather uniform and strongly negative value east of the ice edge. However, this flux

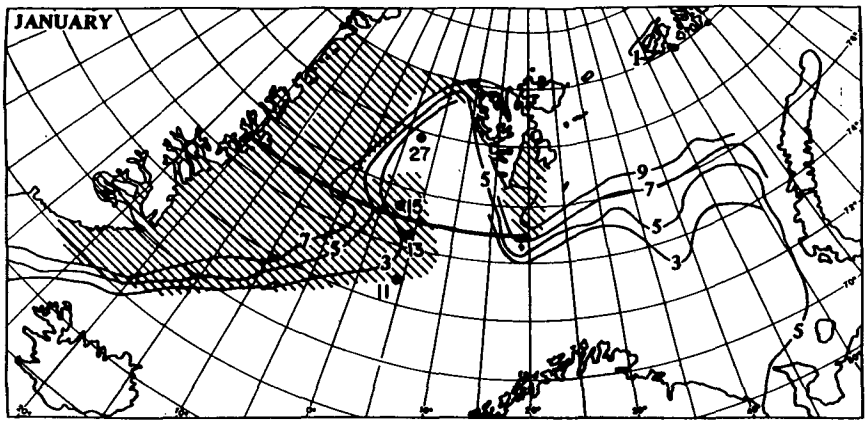

FIG. 2. January mean sea ice distribution (%) in the Greenland Sea over the 1971–80 period (after T. Vinje, 1985). Superimposed as a heavy line is the zonal slab under investigation. Also shown are some positions of stations carried out by CSS *Hudson* and the related ice extent (hatched area) in winter 1982.

increases westward from the ice edge to almost zero, following the ice concentration distribution. In summer, it is also the sensible heat flux which is responsible for the zonal variations of the surface warming except for the rapid decrease in the west due to the oceanic heat loss below the ice cover. Finally, the friction velocity u_* was taken equal to 8×10^{-3} m s^{-1}, a mean value calculated from wind stresses reported by Aagaard (1970) over the Greenland Sea.

The initial state is described by a mean annual stratification based upon Hibler and Bryan analysis (1987). Initial ice concentrations were estimated by examining in the first time step the surface heat budget at all the grid points and compensating for any imbalance by growing ice assuming an early winter initial growth rate of 4 cm day^{-1} (Hibler, 1979). In this initial step, any salt flux created by ice formation was ignored.

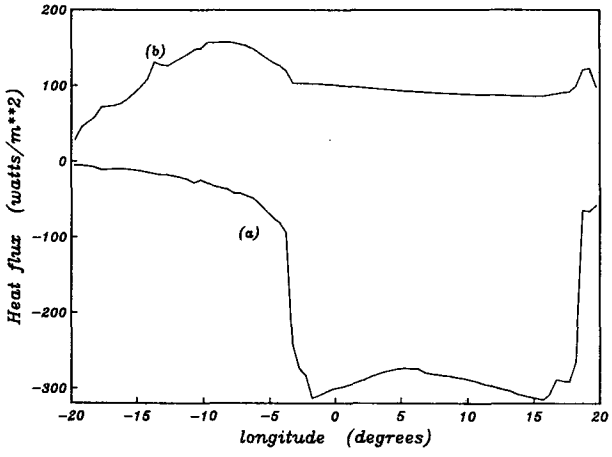

FIG. 3. (a) Winter and (b) summer distributions of the heat gain at the ocean surface (W m^{-2}).

A characteristic of the polar regions is that the heat budget of any point at the ocean surface is globally negative on an annual basis so that heat lost by the ocean to the atmosphere has to come into the system by some advective process. In the Greenland Sea, the oceanic advection is essentially meridional with two main currents, the West Spitzbergen current and the East Greenland current. The resulting effect is to bring heat into the basin from the south. Also, the local salt budget is expected to be nonzero because the Greenland Sea is recognized to be an area of local melting (sink of ice mass for the Arctic): ice transported by the East Greenland current from the Arctic Ocean is responsible, as it melts in the Greenland Sea, for additional fresh water fluxes which are easily identified in the low-salinity surface layer. In order for the model to reach thermodynamic equilibrium, advection effects have been included through the addition of a source term in the temperature and salinity equations, within the mixed layer and at all levels describing the underlying stratification. This term parameterizes a restoring force toward a climatological—in fact, the initial—stratification:

$$S_T = -\frac{1}{C}(T - T_{\text{clim}})$$

$$S_S = -\frac{1}{C}(S - S_{\text{clim}}) \qquad (16)$$

where $C = 3$ years is a constant characterizing the relaxation time scale of the system. Here (T, S) are equal to (T_m, S_m) in the mixed layer and to (T_k, S_k) at any k-level below the mixed layer, and $(T_{\text{clim}}, S_{\text{clim}})$ are the climatological temperature and salinity of the first level in case mixed layer equations are considered, or of the kth level for any k-level below the mixed layer.

The seasonal cycle of the atmospheric forcings ap-

plied in the model is shown in Figs. 4a and 5a at two different locations. One point has been selected in an area of higher ice concentrations and the other one in an open water area. Both curves display variations about an obviously negative annual mean value. The vertically integrated meridional heat and salt fluxes, plotted in the same way in Figs. 4b and 5b undergo variations of smaller amplitude, at least by one order of magnitude, than the atmospheric fluxes. This is not true, however, for the salt flux in ice-covered areas where both atmospheric and meridional fluxes have variations of similar amplitude. Nevertheless, the latter remain small compared with the large salt fluxes induced by ice melting or growth into the surface layer. Therefore, S_T and S_S are expected to have little direct influence on the evolution of the surface layer. Their effect is felt indirectly through the entrainment fluxes in which $T(-h_m)$ and $S(-h_m)$ are now kept close to a climatological stratification. Otherwise, under persistent surface cooling or in absence of any fresh water input they would possibly drift away from realistic values.

In order to obtain a reliable seasonal cycle, the model has been integrated over ten years until the total heat and salt sources entering the system balance each other on an annual basis. At the beginning of the integration, strong heat loss and salt gain occur as the system tends

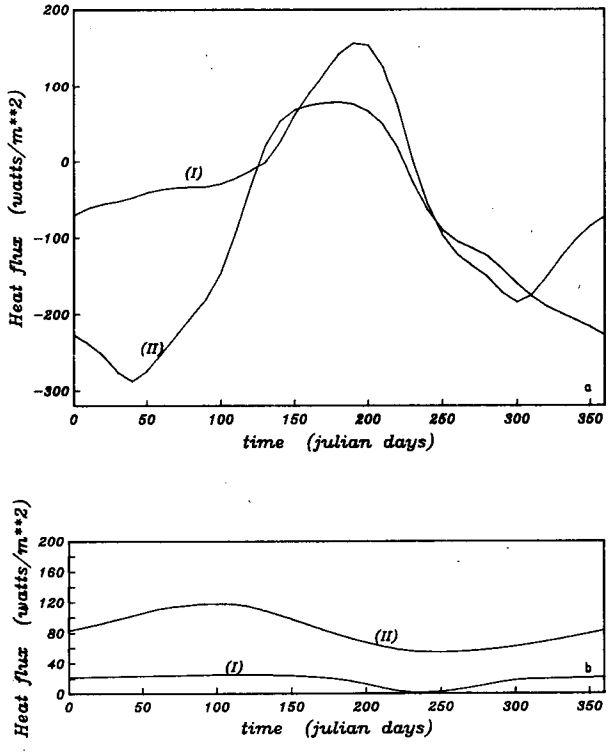

FIG. 4. Annual cycle of (a) the surface atmospheric and (b) lateral heat fluxes (W m^{-2}) at two locations. To be multiplied by 2 in order to get the equivalent buoyancy forcing in 10^{-10} W kg^{-1}: (I) in an ice-covered area (8°W), (II) in open water (5°E).

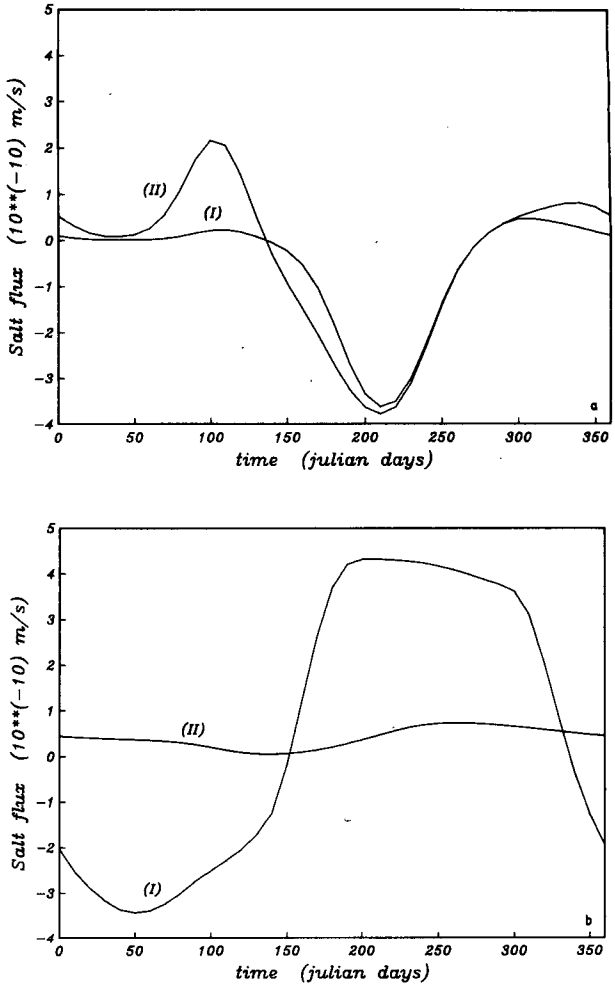

FIG. 5. Annual cycle of the surface atmospheric (a) and lateral (b) salt fluxes (10^{-10} m s^{-1}) at two locations. To be multiplied by 8 in order to get the equivalent buoyancy forcing in 10^{-10} W kg^{-1}: (I) in an ice covered area (8°W), (II) in open water (5°E).

to equilibrate under the surface atmospheric forcing. After three years, the annual heat loss has decreased by one order of magnitude compared to its initial value, and finally after ten years the annual heat and salt source terms oscillate about zero with a relative amplitude of only 1% to 3% compared to their initial values.

b. *Discussion of results*

Figure 6a shows the zonal distribution of the mixed layer in early winter (1 January) and Fig. 7 shows the corresponding vertical distributions of temperature and salinity. Without considering shallow shelf areas on both sides of the basin the pycnocline reaches its minimum depth in the west below the ice (see Fig. 9a for corresponding ice concentrations) with approximate depths of 120–150 m. On the opposite side, values corresponding to open water conditions increase to about

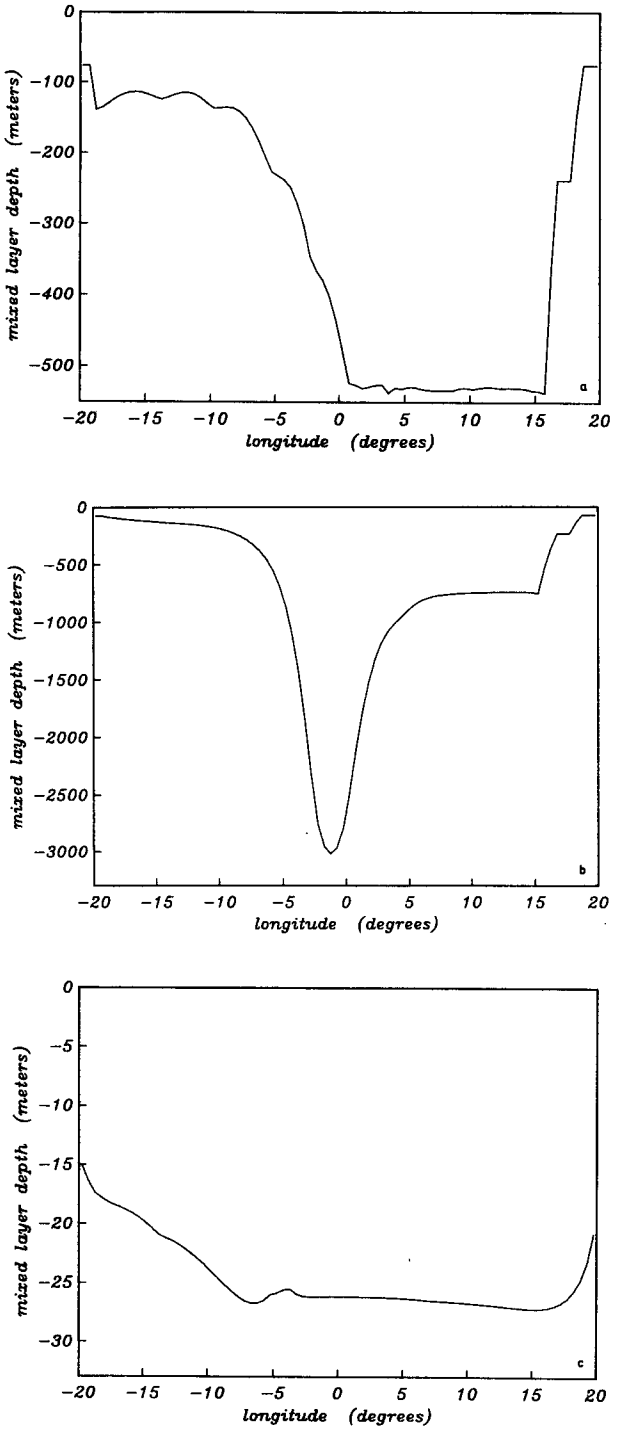

FIG. 6. (a) Early and (b) late winter, and (c) summer mixed-layer depth distributions (m).

500 m. Later on at the end of winter (Fig. 6b), the mixed layer exhibits the greatest thicknesses east of the ice edge, with values reaching 3000 m (bottom depth) in some places. These winter results can be compared with hydrographic data collected by CSS Hudson between 14 February and 6 April 1982 in the Norwegian Sea and more specifically in the Greenland basin. Below the ice, as at Stations 13 and 15 (Fig. 8a), both temperature and salinity are vertically homogeneous over the upper 100–120 m, allowing definition of a fresh and cold mixed layer. This surface layer overlies the warm and salty Atlantic water known to recirculate southward below the polar water. In the central part of the basin, at Station 27 (Fig. 8b), a deeper layer almost mixed over the upper 600 m is found. Finally, farther south (Station 11) a 300 m thick mixed layer which is made of warm and salty water overlying the cold, deep water characterizes the type of stratification encountered on the eastern side of the basin in the inflow of Atlantic water. The model results (Fig. 7) compare well with these observations. However, the available data do not really allow verification of the hypothesis of a penetrative convection like the one predicted in late winter by the model in the central part of the basin. Most of the collected profiles are rather uniform over the upper 600 m both in temperature and salinity, but no real straight line, well-mixed profile has been found. The late winter bottom convection can be compared with the formation of "chimneys" in the Weddell Sea (Gordon, 1978). According to Killworth (1979), without considering any other mechanism than buoyancy-driven vertical mixing catastrophic overturning down to the bottom should have

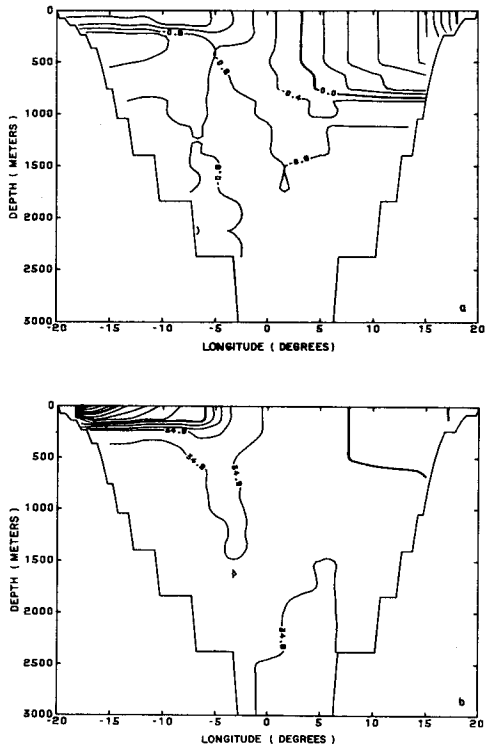

FIG. 7. Winter vertical (a) temperature (°C) and (b) salinity (‰) distributions.

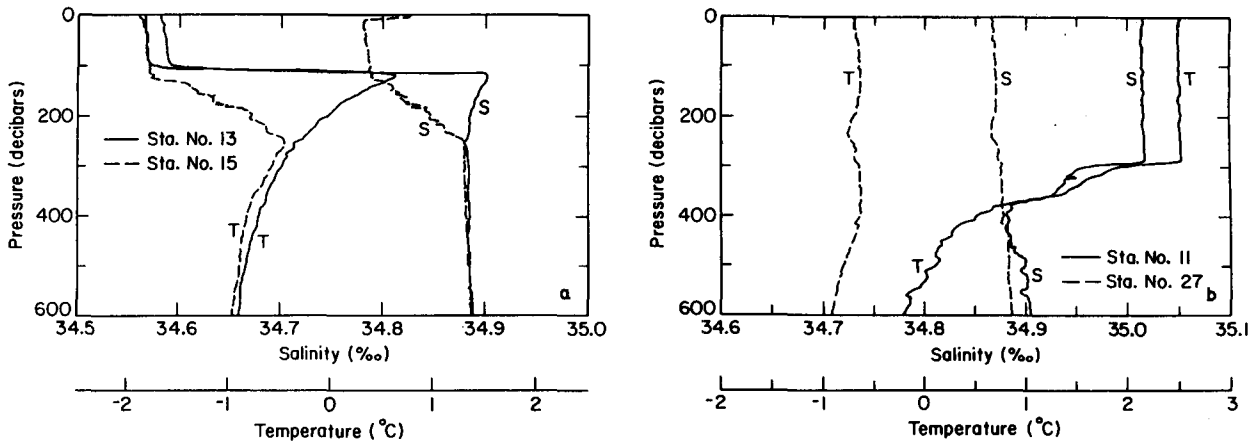

FIG. 8. Typical mixed-layer temperature and salinity profiles obtained from data collected during the CSS Hudson cruise 82-001 at stations located (a) in the ice-covered area and (b) in the ice-free area (redrawn from Clarke et al., 1984).

occurred at most of the stations located in the Weddell Gyre. The same conclusion was drawn from calculations carried out in the Greenland Sea at 74°N, 0°.

Deep convection is expected to occur in areas where the combined effect of an intense surface cooling and a weak stratification prevents surface freezing through a heat exchange with deeper layers. This is one of the feedback mechanisms responsible for strong correlations between the ice concentration and the mixed-layer thickness. An example of such a correlation is provided on the eastern boundary of the basin. Although the global ice distribution essentially follows the zonal variations of the atmospheric temperature (the magnitude of which decreases from west to east), there is still some ice in shallow eastern areas where the mixed-layer deepening is constrained by the bottom topography. By comparing Fig. 9a with the mean ice concentrations reported by Vinje (1985) for the period 1971–80 (Fig. 2), there is evidence of an underestimation of the ice extent by the model. Based on the 30% ice concentration contours, the ice edge at 75°N is more likely located at about 5°E than 5°W, as predicted by the model. Since the predicted locations of the isolines of higher (>50%) concentrations are in good agreement with the climatological maps, the discrepancy has to be found in the shape of the ice edge which in the model is obviously sharper. This is an expected consequence of neglecting ice dynamics and consequently the possible eastward drift of the ice edge. As an example, investigations of the coupled ice–ocean dynamics by Hakkinen (1984) revealed that applying a southeastward wind over a north–south oriented marginal ice zone (ice to the right of the wind) may induce an off-ice drift of the ice edge for sufficient mixed-layer thicknesses (the selected value was 100 m). Inclusion of ice advection in the present study would have resulted in the insulation of additional portions of the ocean surface from atmospheric cooling which is still very efficient in the center of the basin, and consequently in the partial inhibition of the underlying convective process.

In summer, the situation changes drastically as the mixed layer retreats to a new equilibrium depth under the effect of surface atmospheric heating or fresh water supply from the melting ice (Fig. 6c). The mean equilibrium summer thickness is influenced by the dissipation scale h_w of the mechanical energy input (the only remaining source of turbulence) and by the magnitude of the surface buoyancy flux. The order of magnitude of h_m is about 20 m and is generally higher than the thickness of the top layer which coincides with the first level of the model (15 m). Below the ice, the retreat equilibrium depth compares well with observations, and in particular with MIZEX 84 data (Foster et al., 1985). Since u_* is assumed uniform over the domain, the zonal variation of the pycnocline level has to be created by a differential buoyancy flux supplied by heat and salt sources: melting seems to be a more efficient mechanism than surface heating in contributing to the restratification of the surface layer.

In addition, summer ice concentrations (Fig. 9b) are very low, with most of the ice confined west of 15°W, a distribution which differs significantly from observations made in this area (Vinje, 1985). A solution to this problem is not provided by inclusion of ice dynamics since Hibler and Bryan (1987) with both ice and ocean dynamics considered in their model have similarly obtained an almost ice free Greenland basin in summer. On the other hand, an explanation is to be found in simplification allowed in ice thermodynamics. In the present model, a constant value of 2 meters for the ice thickness is probably an overestimation in summer when both ice thickness and concentration are likely to decrease simultaneously. According to Maykut (1984), the rate of lateral melting in leads is expected to increase with the area of open water, the narrower the lead, the higher the rate of increase. Therefore the present model, in which the

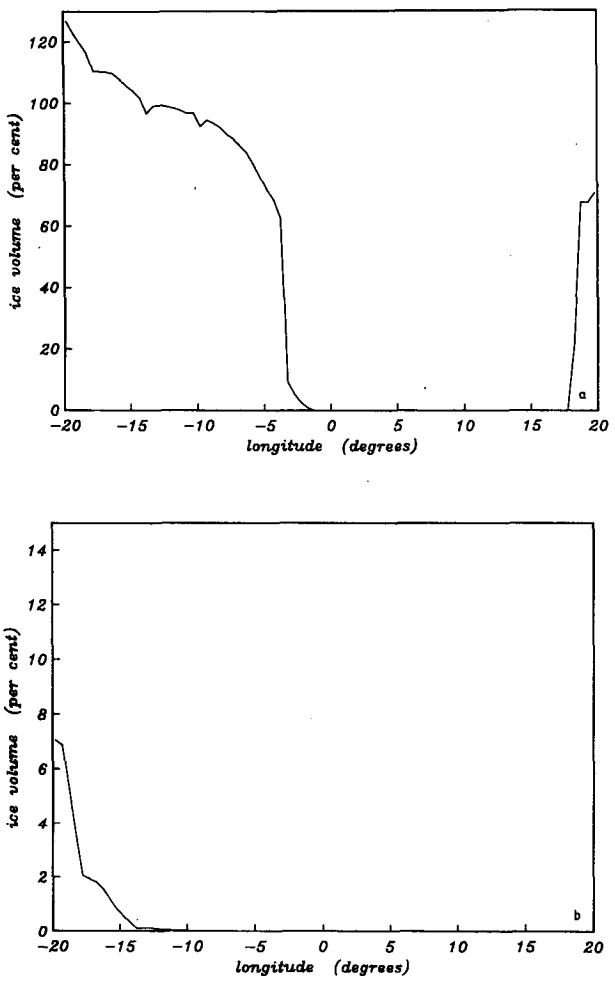

FIG. 9. (a) Winter and (b) summer sea ice distributions (percentage of ice volume). Percentages are relative to a reference volume of same horizontal section and H_0 = 2 m height. Values higher than 100% indicate ice thicknesses greater than 2 m.

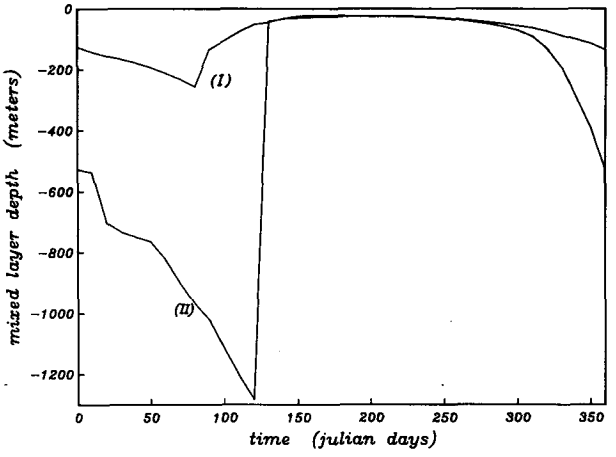

FIG. 10. Annual cycle of the mixed-layer depth (m) at two locations: (I) in an ice-covered area (8°W) and (II) in open water (5°E).

volume of melted ice is not shared in compactness and thickness changes, does underestimate the ice concentration during the decay phase and doing so enhances the effect of the lateral melting. Similarly in Hibler and Bryan (1987) ice thermodynamics, although more elaborate, is highly parameterized using only two ice-thickness levels. In addition, although the ocean in their study appears to play a minor role in the ice decay phase, one can expect that inclusion of overturning in the underlying ocean, which as said earlier can be very active in winter east of the ice edge, enhances melting effects during the following summer.

The seasonal evolution of the mixed-layer thickness at two locations is plotted in Fig. 10: grid point I is located on the west side in an ice-covered area and grid point II is in open water. Also shown is the corresponding evolution of the ice concentration at point I (Fig. 11). At both locations maximum pycnocline depths are reached in late winter (day 110) somewhat earlier below the ice, just before mixed-layer retreat is triggered. Minimum equilibrium values for h_m are found when the ice concentration reaches its minimum (point I) or when the surface heat flux reaches its maximum (point II). The rapid retreat is a result of the diagnostic estimation of h_m regardless of the mixing history evidenced in the previous values of h_m. There is no observational evidence for this kind of behavior: in the MEDOC deep convection area, the retreat was found to occur primarily as a result of horizontal processes like interleaving, none of which can be included in the context of a one-dimensional model. On the other hand, the rapid mixed-layer deepening occurring in the fall follows from a prediction of the entrainment rate by the model and is consequently more reliable. In some places it could be the signature of a catastrophic overturning similar to the one obtained in the Weddell Sea where values of 180 to 300 m were the limit depths

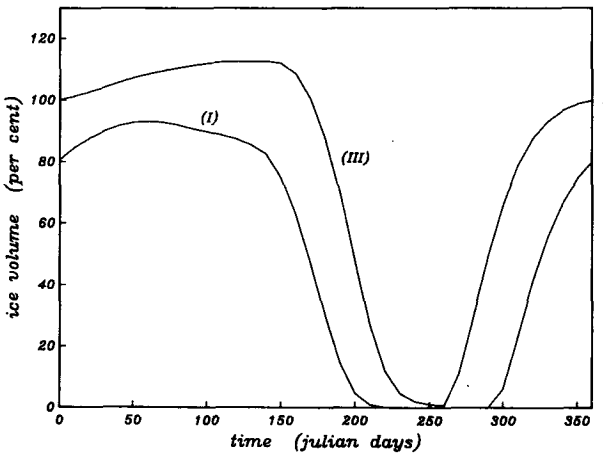

FIG. 11. Annual cycle of the percentage of ice volume at two locations: (I) in a seasonally ice-covered area (8°W) and (III) in a permanently ice-covered area (15°W).

for the mixed layer beyond which overturning occurred down to the bottom. Comparison between Figs. 10 and 11 demonstrates that, as soon as surface freezing is initiated (point I), the entrainment velocity is greatly reduced compared with open water areas (point II). Brine rejection from growing ice is therefore less efficient in driving convective mixing than surface cooling.

Minimum ice concentrations are found in late August and maximum in early March (Fig. 11). Ice growth starts as early as September in high-concentration areas where the mixed layer has not been too affected by summer warming, and as late as November in areas where ice totally disappears in summer. In this case, the mixed layer has to be intensely cooled from the surface as entrainment tends to bring some heat from below, before the surface temperature reaches the freezing point. The higher the summer mixed-layer temperature, the larger the time lag between the initiation of the mixed-layer deepening and the ice growth.

Comparison between Figs. 4a, 10 and 11 shows how ice–ocean interaction is important in coordinating the different annual cycles. Entrainment is responsible for the onset of ice melting which has to have lasted for a few weeks before the fresh water thus released is able to trigger the retreat of the mixed layer. Subsequent increase of the melting rate occurs when surface heating starts in early May. Contrarily, the combined effects of mixed-layer deepening and surface cooling determine the time when surface freezing can start.

The stronger seasonal signal in temperature is found in eastern areas where the negative atmospheric heat flux in summer leads to a well-marked temperature maximum in early September (Fig. 12). In western ice-covered areas the amplitude of the seasonal temperature cycle is not so large, since minimum values are limited by surface freezing. On the other hand, a strong salinity minimum is found in summer (Fig. 13) which

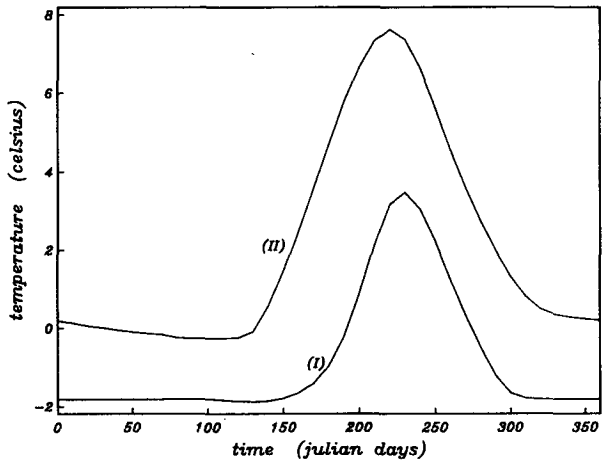

FIG. 12. Annual cycle of the mixed-layer temperature (°C) at two locations: (I) in an ice-covered area (8°W) and (II) in open water (5°E).

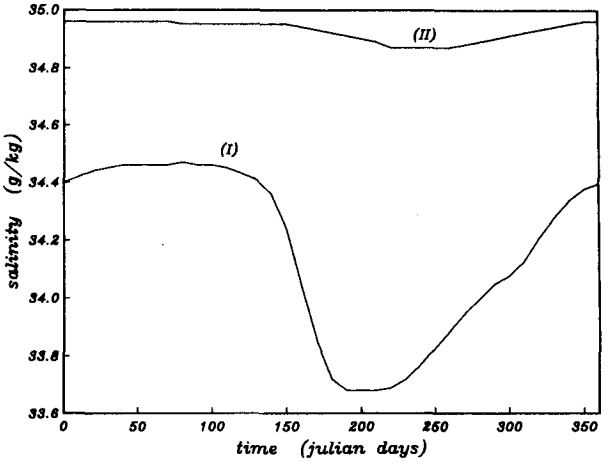

FIG. 13. Annual cycle of the mixed-layer salinity (‰) at two locations: (I) in an ice-covered area (8°W) and (II) in open water (5°E).

does not occur in open water, but the tendency is reversed well before ice growth is initiated: the surface salinity starts to increase just after entrainment is triggered (day 180), bringing some salt from the deeper layers. Later on brine rejection from growing ice participates in the increase of the surface salinity. The decrease of the mixed-layer temperature occurs simultaneously but is stopped very soon by freezing. Only areas with relatively high ice concentrations reach the freezing point. Even for maximum ice concentrations as high as 70%, the mixed-layer temperature is slightly above the freezing point.

The heat content of the mixed layer is an important factor which, according to (13), determines the magnitude of the oceanic heat flux to the ice. Allowing the mixed layer to be above the freezing point in many cases limits the amount of heat released to the ice. The mixed-layer heat content is influenced by entrainment and surface forcing, both having their signature in the annual cycle of the heat flux F_{WI} (Fig. 14). This flux has an intermittent behavior characterized by two peaks: one occurs at the period of more active melting (June–July) when the surface layer is absorbing heat from the atmosphere in open water, and the other one corresponds to the time of rapid deepening of the mixed layer (December). The annual mean value is one order of magnitude higher than the value usually conceded for this flux in the central Arctic (2 W m^{-2}, see Maykut and Untersteiner, 1971). It has to be regarded as representative of deep convection areas where the entrained heat flux plays a prominent role.

4. Conclusion

The preceding results illustrate the ability of the present coupled ice–mixed-layer model to simulate the seasonal cycle of the vertical mixing processes in areas like the Greenland Sea, characterized by intense surface

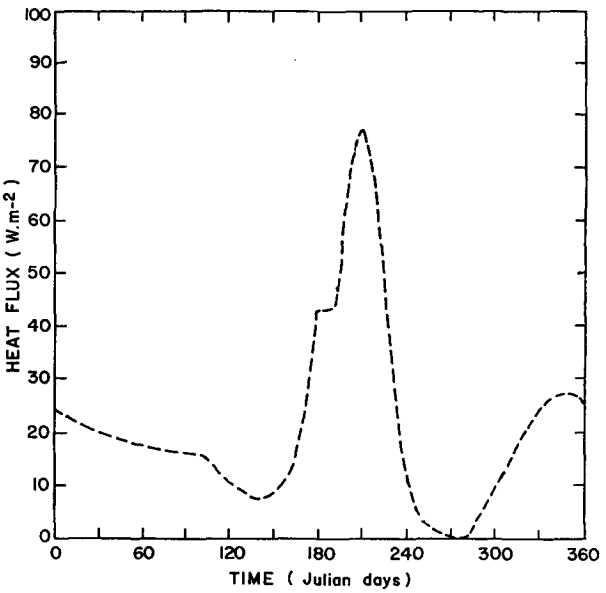

FIG. 14. Annual cycle of the oceanic heat flux (W m^{-2}) at the bottom of the ice at 15°W.

cooling and ice formation. According to observations, the surface layer was assumed equally mixed with regard to both heat and salt; vertically integrated conservation equations have been used to calculate its temperature and salinity. Buoyancy effects together with mechanical mixing have been considered in the entrainment equation with different dissipation rates depending on the mixed-layer thickness and on the subsequent prevailing source of turbulence. Two types of temperature and salinity profiles have been evidenced, 1) below the ice a fresh and cold mixed layer and 2) in open water a warm and salty mixed layer. The entrainment velocity also depends crucially upon the density gradient across the pycnocline, and consequently upon the temperature and salinity immediately below the mixed layer. In order for the system to reach thermodynamic equilibrium, deep temperatures and salinities were forced to remain close to climatological values through a restoring force with a relaxation time constant of 3 years. Potential energy, heat and salt are conserved during both entrainment and retreat phases. These conservative properties are an interesting feature of the model, especially when applied to the potential energy of the whole vertical T–S profile: the model provides a fairly accurate estimation of the variations of the pycnocline shape which are of particular importance in the stratified waters encountered below the ice.

The large horizontal variations of the mixed-layer thickness in winter are consistent with Lemke and Manley (1984), who concluded that the surface mechanical wind or ice stress accounts only for one third of the mixing energy in winter. The effect of the surface stress, assumed here to be spatially uniform, is negligible compared to the buoyancy effects. Also, surface cooling is recognized to be a more efficient source of turbulence than brine rejection. The model performance for predicting mixed-layer characteristics are better in winter than in summer for two reasons. First, like most bulk-layer models the present one suffers from a poor description of the retreat process. Second,

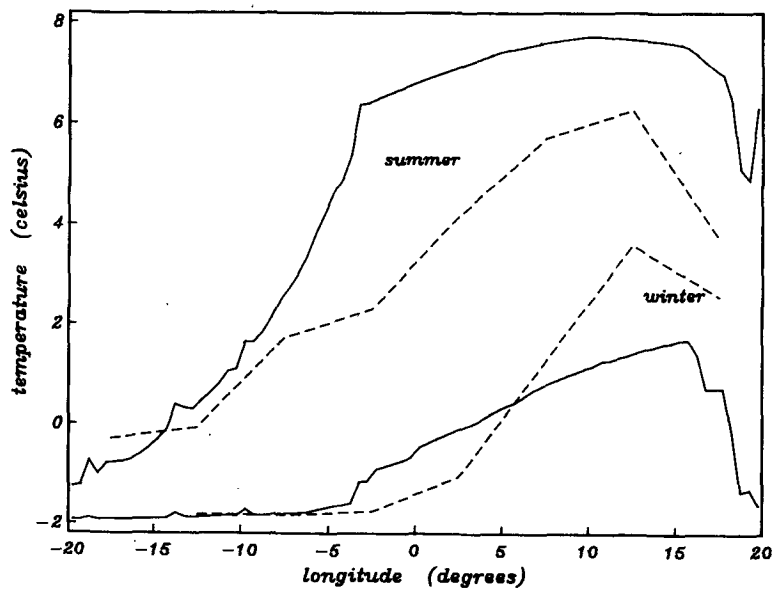

FIG. 15. Winter and summer distributions of the mixed-layer temperature (°C). Also plotted as dashed lines are the 3-month averages of the observed surface temperatures along the same latitude circle.

the amount of fresh water supplied from the melting ice is underestimated because meridional ice advection has not been accounted for. As a direct consequence, the mixed-layer salinity in summer is too high below the ice with minimum values of about 32‰, instead of values of 30‰ which are commonly found.

Mixed-layer models are usually evaluated in view of their ability to accurately predict the ocean surface temperature. The zonal distribution of the summer and winter mixed layer temperatures have been plotted in Fig. 15, together with the corresponding observed climatological temperatures (Houssais et al., 1987). Model temperatures when compared to observations are globally higher in summer and lower in winter but the shape of the zonal profiles is very similar. Since climatological values are based upon a 3-month time averaging of data centered respectively about day 220 and day 40, it is possible that such an averaging process tends to reduce the amplitude of the seasonal contrast.

The thermodynamic ice model forced by interactive oceanic heat flux and by prescribed atmospheric fluxes provides acceptable results for ice concentrations in

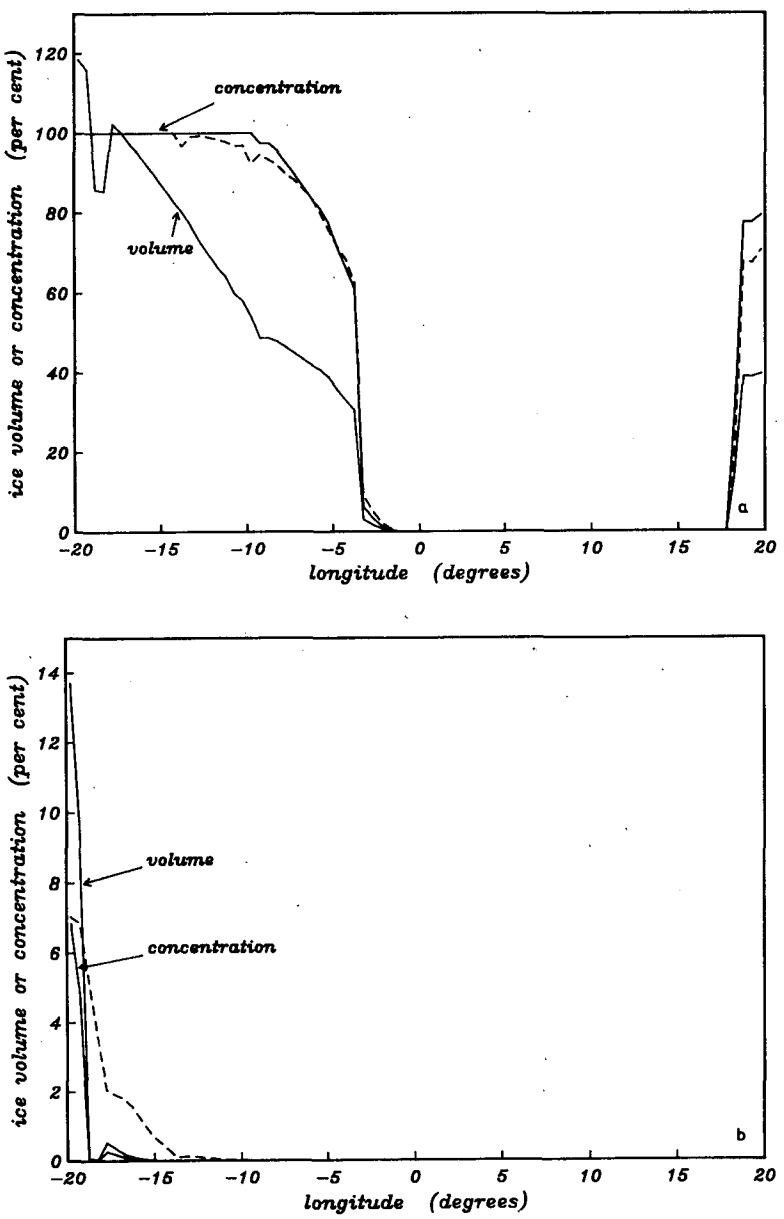

FIG. 16. (a) Winter and (b) summer sea ice distributions expressed in percentages of both ice volume (as in Fig. 9) and ice-covered area (concentration A) for the case $H_0 = 1$ m, $k_I = 2$ W K^{-1} m^{-2}. Also shown as a dashed line is the corresponding ice concentration distribution for the standard case ($H_0 = 2$ m).

winter but definitely too low in summer. As discussed earlier, the simplified thermodynamics is probably responsible for this problem. In order to test the sensitivity of the model to the prescribed value assigned to the ice thickness H_0, another numerical experiment was carried out setting $H_0 = 1$ m. Results for the ice concentration and ice volume distributions are presented in Fig. 16. The percentages of ice volume are still calculated relative to the same reference volume (2 m^3). In winter, the ice volumes are smaller than in the standard case ($H_0 = 2$ m) but the ice concentrations are about the same. This means that ice thicknesses are globally smaller even for 100% ice concentrations. In summer the situation is reversed, since now similar ice-volume distributions correspond to different ice concentrations: the western part of the basin exhibits higher ice concentrations for smaller H_0. Therefore, in terms of ice concentrations (the parameter which actually determines the ocean surface forcing), the model seems to be sensitive in summer to the assumed ice thickness. The differences obtained both in summer and winter demonstrate the necessity for a more sophisticated parameterization of ice thermodynamics, taking into account some multilevel ice-thickness distribution (Hibler, 1979; Thorndike et al., 1975).

The ice concentration is also sensitive to the heat flux coming from the ocean. This flux was found to be particularly large in periods of mixed-layer deepening or surface heating. Its parameterization is expected to have important consequences on the equilibrium ice distribution. In particular, conversion into latent heat of melting of part of the mixed-layer heat content in order for its temperature to remain at the freezing point would lead to a considerable decrease of the ice concentration over the entire year.

The one-dimensional processes investigated in the present study can explain to a significant extent the seasonal evolution of the ocean surface stratification in relation with the atmospheric or ice forcing. Nevertheless, ocean advection which has been poorly stimulated here by the addition of a source term in the temperature and salinity equations may play an important role in the horizontal redistribution of the pycnocline topography and mixed-layer characteristics. The prediction of the velocities in the surface boundary layer in relation to realistic wind or ice-stress fields would improve the prediction of the summer mixed layer by an adequate estimation of the mechanical sources of turbulence especially when the mixed layer retreats to shallow levels. A differential surface stress, like the one found at the ice edge discontinuity, can induce vertical motions which are evidenced in the horizontal variations of the mixed-layer thickness (Johannessen et al., 1983). Simultaneously, ice advection seems to play a major role in the estimation of the ice concentration field. Meridional ice advection is responsible for a net fresh water supply into the marginal ice zone, while zonal advection can result in the redistribution of the ice concentration field. In particular, the eastward drift of the ice edge can significantly modify the local surface heat and salt budgets. The investigation of these processes requires one to introduce ice dynamics in the model, eventually including the internal ice stresses which can modify the horizontal distribution of the ice velocity (Leparranta and Hibler, 1985).

Acknowledgments. We would like to thank Dr. W. D. Hibler III for his useful comments on this paper. Dr. Patrice Klein was very helpful by making thoughtful criticisms. We also thank Jackie Castor for the rapid word processing of the manuscript, Ed Perkins for the careful preparation of the figures, and Steve Bowen for editing assistance.

This work was supported by the Centre National de la Recherche Scientifique, through the P.N.E.D.C. ASP IOGA, and partly by the U.S. Army European Research Office, Contract DAJA45-85-M-0383, via a reimbursable Office of Naval Research grant through the U.S. Army Cold Regions Research and Engineering Laboratory. Computing support was provided by the Conseil Scientifique du Centre de Calcul Vectoriel pour la Recherche in Palaiseau and by the Centre Interrégional de Calcul Electronique du CNRS.

REFERENCES

Aagaard, K., 1970: Wind-driven transports in the Greenland and Norwegian Seas. *Deep-Sea Res.*, **17**, 281–291.

Adamec, D., R. L. Elsberry, R. W. Garwood and R. L. Haney. 1981: An embedded mixed-layer ocean circulation model. *Dyn. Atmos. Oceans*, **6**, 69–96.

Carmack, E. C., and K. Aagaard, 1973: On the deep water of the Greenland Sea. *Deep-Sea Res.*, **20**, 687–715.

Clarke, R. A., J. L. Reid and J. H. Swift, 1984: CSS *Hudson* cruise 82-001, 14 February–6 April 1982. Vol. 2, CTD data plots. Data Rep. No 84–14, Scripps Institution of Oceanography, University of California, 172 pp.

Foster, T. D., B. S. McNamara, T. M. Bandurraga and E. G. Eckert, 1985: Physical oceanographic data, Marginal Ice Zone Experiment. R/V Polarqueen, June–July 1984. Report, University of California, Santa Cruz.

Gascard, J. C., and R. A. Clarke, 1983: The formation of Labrador Sea water. Part II: Mesoscale and smaller scale processes. *J. Phys. Oceanogr.*, **13**, 1779–1797.

Gordon, A. L., 1978: Deep Antarctic convection west of Maud Rise. *J. Phys. Oceanogr.*, **8**, 600–612.

Hakkinen, S., 1984: Dynamics of the coupled ice–ocean system in the marginal ice zone: Study of the mesoscale processes and of constitutive equations for sea ice. Ph.D. dissertation, Florida State University, Tallahassee.

Hibler, W. D. III, 1979: A dynamic thermodynamic sea ice model. *J. Phys. Oceanogr.*, **9**, 815–846.

——, 1980: Modeling a variable thickness sea ice cover. *Mon. Wea. Rev.*, **108**, 1943–1973.

——, and K. Bryan, 1987: A diagnostic ice–ocean model. *J. Phys. Oceanogr.*, **17**, 987–1015.

Houssais, M. N., J. Raunet and J. C. Gascard, 1987: *Hydrographic Atlas of the Greenland Sea.* In press.

Johannessen, O. A., J. A. Johannessen, J. Morison, B. A. Farrelly and E. A. S. Svendsen, 1983: The mesoscale oceanographic conditions in the marginal ice zone north of Svalbard in early fall 1979. *J. Geophys. Res.*, **88**, 2755–2769.

Killworth, P. D., 1979: On "chimney" formations in the ocean. *J. Phys. Oceanogr.*, **9,** 531–554.

Kim, J. W., 1976: A generalized bulk model of the oceanic mixed layer. *J. Phys. Oceanogr.*, **6,** 686–695.

——, and W. L. Gates, 1980: Simulation of the seasonal fluctuation of the upper ocean by a global circulation model with an embedded mixed layer. Rep. No. 11, Climatic Research Institute, Oregon State University, 60 pp.

Kraus, E. B., and J. S. Turner, 1967: A one-dimensional model of the seasonal thermocline, Part II. *Tellus,* **19,** 98–106.

Lepparanta, M. and W. D. Hibler III, 1985: The role of plastic ice interaction in the Marginal Ice Zone dynamics. *J. Geophys. Res.,* 11 899–11 909.

Lemke, P., and T. O. Manley, 1984: The seasonal variation of the mixed layer and the pycnocline under polar sea ice. *J. Geophys. Res.*, **89,** 6494–6504.

Manabe, S., and R. J. Stouffer, 1980: Sensitivity of a global climate model to an increase of CO_2 concentration in the atmosphere. *J. Geophys. Res.*, **85,** 5529–5554.

Martinson, D. G., P. D. Killworth and A. L. Gordon, 1981: A convective model of the Weddell Polynya. *J. Phys. Oceanogr.*, **11,** 466–488.

Maykut, G. A., 1984: On the decay and retreat of the ice cover in the summer MIZ. *MIZEX Bulletin,* **III,** 15–22.

——, and N. Untersteiner, 1971: Some results of a time-dependent thermodynamic model of sea ice. *J. Geophys. Res.*, **76,** 1550–1575.

Mellor, G. L., and T. Yamada, 1982: Development of a turbulence closure for geophysical fluid problems. *Rev. Geophys. Space Phys.* **20,** 851–875.

Metcalf, W. G., 1955: On the formation of bottom water in the Norwegian Basin. *Trans. Amer. Geophys. Union,* **36,** 595–600.

Niiler, P. P., and E. B. Kraus, 1977: One-dimensional models of the upper ocean. *Modeling and Prediction of the Upper Layers of the Ocean,* Chapter 10, E. B. Kraus, Ed., Pergamon, 143–172.

Parkinson, C. L., and W. M. Washington, 1979: A large-scale numerical model of sea ice. *J. Geophys. Res.*, **84,** 311–337.

Pollard, R. T., P. B. Rhines and R. Thompson, 1973: The deepening of the wind-mixed layer. *Geophys. Fluid Dyn.*, **3,** 381–404.

Pollard, D., M. L. Batteen and Y. J. Han, 1983: Development of a simple upper-ocean and sea-ice model. *J. Phys. Oceanogr.*, **13,** 754–768.

Robinson, M. K., R. A. Bauer and E. H. Schroeder, 1979: Atlas of North Atlantic–Indian Ocean monthly mean temperatures and mean salinities of the surface layer. Naval Oceanogr. Off., Ref. Publ. 18.

Roed, L. P., 1984: A thermodynamic coupled ice–ocean model of the Marginal Ice Zone. *J. Phys. Oceanogr.*, **14,** 1921–1929.

——, and J. J. O'Brien, 1983: A coupled ice–ocean modeling of upwelling in the Marginal Ice Zone. *J. Geophys. Res.*, **88,** 2863–2872.

Solomon, H., 1973: Wintertime surface layer convection in the Arctic Ocean. *Deep-Sea Res.*, **20,** 269–283.

Thorndike, A. S., D. A. Rothrock, G. A. Maykut and R. Colony, 1975: The thickness distribution of sea ice. *J. Geophys. Res.*, **80,** 4501–4513.

Vinje, T., 1985: Sea Ice distribution 1971–1980. Norsk Polar Institutt Skrifter N. 179c, Oslo.

Vowinckel, E., and S. Orvig, 1970: The climate of the North Polar Basin. *World Survey of Climatology, V. 14: Climates of the Polar Regions,* S. Orvig, Ed., Elsevier: 370 pp.